TRANSPORTATION RESEARCH BOARD
NATIONAL RESEARCH COUNCIL

IDEA

Innovations Deserving Exploratory Analysis Project

NATIONAL COOPERATIVE HIGHWAY RESEARCH PROGRAM

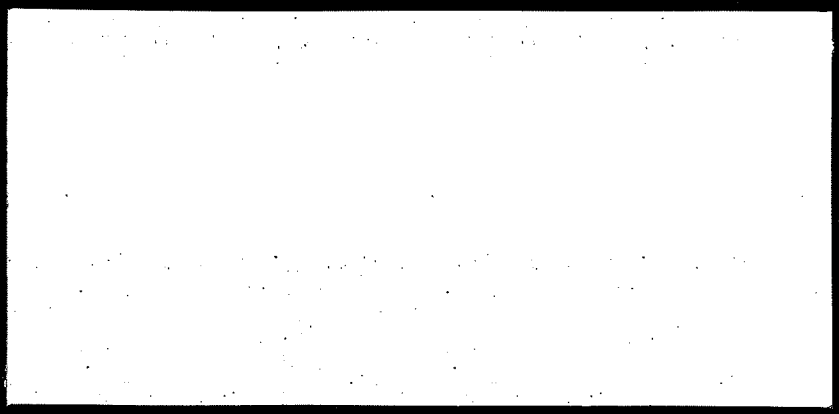

Report of Investigation

IDEA PROJECT FINAL REPORT
Contract NCHRP-94-ID012

IDEA Program
Transportation Research Board
National Research Council

September 1995

ADVANCED TESTING OF AN AUTOMATED NDE SYSTEM FOR HIGHWAY PAVEMENT SURFACE CONDITION ASSESSMENT

Prepared by:
Sidney A. Guralnick and Eric S. Suen
Advanced Building Materials and Systems Center
Illinois Institute of Technology

INNOVATIONS DESERVING EXPLORATORY ANALYSIS (IDEA) PROGRAMS
MANAGED BY THE TRANSPORTATION RESEARCH BOARD (TRB)

This NCHRP-IDEA investigation was completed as part of the National Cooperative Highway Research Program (NCHRP). The NCHRP-IDEA program is one of the four IDEA programs managed by the Transportation Research Board (TRB) to foster innovations in highway and intermodal surface transportation systems. The other three IDEA program areas are Transit-IDEA, which focuses on products and results for transit practice, in support of the Transit Cooperative Research Program (TCRP), Safety-IDEA, which focuses on motor carrier safety practice, in support of the Federal Motor Carrier Safety Administration and Federal Railroad Administration, and High Speed Rail-IDEA (HSR), which focuses on products and results for high speed rail practice, in support of the Federal Railroad Administration. The four IDEA program areas are integrated to promote the development and testing of nontraditional and innovative concepts, methods, and technologies for surface transportation systems.

For information on the IDEA Program contact IDEA Program, Transportation Research Board, 500 5th Street, N.W., Washington, D.C. 20001 (phone: 202/334-1461, fax: 202/334-3471, http://www.nationalacademies.org/trb/idea)

TABLE OF CONTENTS

EXECUTIVE SUMMARY

The purpose of this research was to field test a prototype automated road inspection system. The results of this comprehensive testing are discussed in this report, along with improvements previously made to the system based on these results. This economical, high-speed road inspection system was developed to detect out-of-plane roadway surface distress. The system uses the shadow moiré method and measures both vertical surface displacement and changes in slope of surface distress. Both these parameters are important in determining the severity of certain types of roadway surface distress.

Unlike traditional methods of road inspection, in which a lane of a roadway is closed temporarily and inspectors walk along the roadway to search for surface distress, the automated road inspection system relies on video and distance tracking systems housed in a moving vehicle. The prototype road inspection vehicle used in this research was an enclosed uni-axle trailer, which can acquire road surface distress information at speeds in excess of 88 km/hr (55 mi/hr). Because the system is automated, only two individuals are needed to drive the towing vehicle and trailer and to operate the data acquisition equipment. This type of road inspection procedure eliminates the need for lane closures and leads to safety levels greater than those achieved with traditional road inspection methods.

Roadway surface distress information is acquired by means of the shadow moiré method. This method uses special white light emitters and a grating, a system of parallel wires, to establish a shadow moiré interferogram. A rectangular opening on the trailer floor houses the grating; four light emitters are mounted above it. An interferogram, which results from the geometrical interference between the wires of the grating and their shadows on the road surface, is created within the area of the grating. The interferogram produces a fringe pattern, a system of dark black bands separated by a light background. These fringe patterns are recorded onto high-resolution videotape by means of a closed circuit display (CCD) video camera housed inside the trailer. The videotape is analyzed later at a postprocessing facility, in which image processing equipment extracts information on the condition of the roadway.

This research focused both on improving shadow moiré road inspection technology and producing a comprehensive, user-friendly software package to assess road surface distress. Improvements resulting from this research include a 22 percent increase in maximum vehicle acquisition speed, new light emitters with special horizontal condenser lenses to improve fringe pattern contrast, a single lightweight grating as opposed to two smaller gratings for greater road coverage, and a more accurate distance measuring system. Refinements in postprocessing include rewriting C-based image analysis algorithms so that they run under the Pentium personal computer processor instead of video processors, which are slower. Improvements in image digitization also were realized, such as better image data integrity and large increases in throughput, allowing for faster postprocessing of videotape images.

IDEA PRODUCT

An inexpensive automated road inspection vehicle was developed and tested using the shadow moiré optical interference method. The vehicle can acquire road surface distress information at velocities of approximately 88 km/hr (55 mi/hr), allowing users to determine, categorize, and rate locations of all out-of-plane surface deformations along a roadway. Unlike traditional methods, in which a lane of a roadway is closed temporarily and inspectors subjectively rate surface distress, the automated road inspection vehicle eliminates the need for road closure and ensures a higher level of safety for its operators. Because the automated road inspection system comprises both computer and image processing equipment, objective and accurate surface distress ratings are realized (*1*). The use of shadow moiré techniques instead of laser technology has resulted in a $60,000 road inspection system, which is more affordable than current commercial laser-based systems. It is anticipated that relatively small road maintenance organizations finally will have the opportunity to acquire such a system, thus improving overall road inspection accuracy and efficiency. The road inspection vehicle is shown in Figure 1.

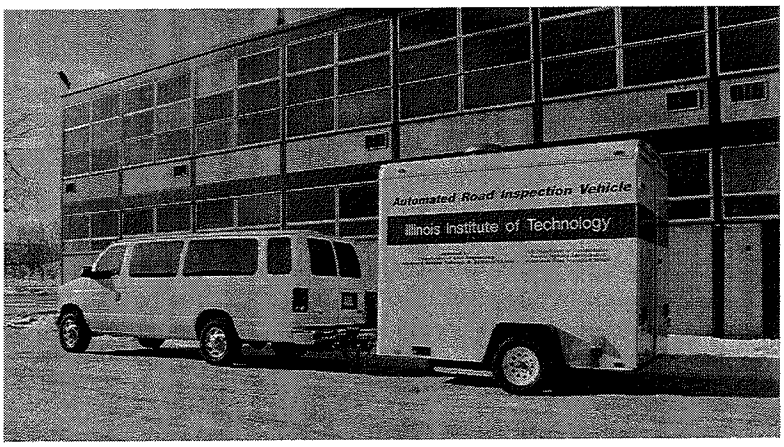

FIGURE 1 Road inspection vehicle.

CONCEPT AND INNOVATION

The shadow moiré-based road inspection system permits continuous, full-field mapping of roadways at highway velocities. Unlike laser-based road inspection systems that reveal data only for a few discrete points along a transverse section, the shadow moiré-based system allows for full-field data acquisition. Images of interferograms along the videotape comprise 512 × 480 pixels, thereby creating approximately 245,000 data points that can be analyzed. The concept of developing an affordable, full-field road inspection system required a simple but accurate means of data acquisition. The shadow moiré method was selected as the most cost-effective means of acquiring full-field surface distress information.

The concept of a mobile shadow moiré system was developed and integrated into a prototype road inspection vehicle in an Illinois Institute of Technology laboratory. The road inspection vehicle comprises a uni-axle enclosed trailer and a van. Other versions of the described road inspection vehicle may include a single vehicle, such as a small recreational vehicle. Video acquisition and recording occurs within the confines of the van, along with precise tracking of the distance traveled by the inspection system. Such tracking information is required to map where each surface distress is located along the roadway. The actual shadow moiré interferometry occurs inside the trailer, where a special frame is installed to mount the required electrical equipment. The trailer floor was modified to accommodate a single large grating that is mounted facing the road surface. A powerful lighting system, using custom-designed line-type condenser lenses, provides the means for the production of the shadow moiré interferograms. Two CCD video cameras in the trailer are used for interferogram capture and general operation monitoring.

MATHEMATICAL BASIS OF SHADOW MOIRÉ METHOD

The mathematical basis of the shadow moiré method is that if two superimposed systems of lines are spaced closely enough and aligned properly, they may form an optical pattern known as a moiré pattern. Such a system of lines may be composed of a group of parallel strands. This kind of system is called a grating. If two gratings are superimposed so that their strands are parallel and white light from a line source is directed on the grating so that the plane of the light is parallel to the strands, then a moiré interference pattern results (*2*) (Figure 2). If only one grating located a small distance from a surface is used with the light source, the shadows of the grating strands are projected onto that surface. The shadow of the grating on the surface, referred to as a virtual grating, may be deformed because a surface may not be completely smooth and plane; hence, the shadows of the grating strands may not be linear. This configuration of a grating and its deformed shadow is the basis of shadow moiré interferometry (*3*). Such a configuration will produce a moiré interferogram, in which fringes will appear in various patterns within the area of the grating. Moiré fringe patterns occur when the distance from the grating plane to a surface is not constant. Elevations or depressions in the surface plane result in deformed shadows of the grating on the surface, thus creating contour lines or fringes (*4*). Fringes, therefore, are optical patterns in which each fringe represents all points of equal distance from the grating plane to the surface.

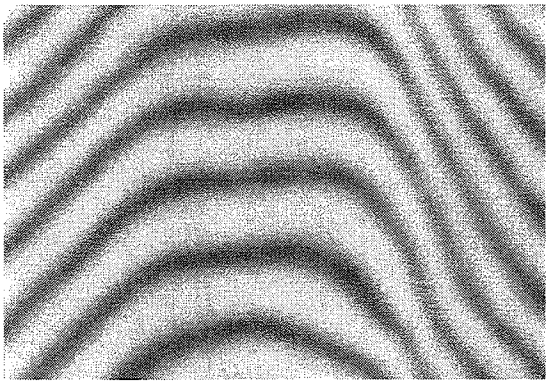

FIGURE 2 Shadow moiré interferogram image.

The general equation for the geometric interpretation of the shadow moiré method follows. In Figure 3, a camera, light source, grating, and surface combine to make a typical shadow moiré system. In this figure, the following are defined:

- The camera or observer position, *O*;
- The light source position, *S*;
- The shadow of the grating in contact with the surface and grating plane, point *a*; and
- *N* fringes, observed at point *d* on the grating and on the surface at point *f*.

Because *N* fringes are observed at point *f* on the surface through point *d* on the grating, the fringes are the result of the interference between the light rays in line *ad* of the grating and those in *ab*, as projected on *af*, on the surface. If the number of light rays in *ad* and *ab* are *m* and *n*, respectively,

$$ad = mp, \quad ab = np$$

hence

$$bd = ad - ab = (m - n)p = Np \tag{1}$$

In Δcdf

$$cf = w \tag{2}$$

$$\angle cfd = 180° - \beta' - (90° + \gamma) = 90° - \beta' - \gamma \tag{3}$$

$$\angle cdf = \beta' \tag{4}$$

because

$$\frac{cd}{\sin(\angle cfd)} = \frac{cf}{\sin(\angle cdf)}$$

therefore

$$cd = \frac{cf \ \sin(\angle cfd)}{\sin(\angle cdf)} \tag{5}$$

Substituting equations (2) through (4) into equation (5)

$$cd = \frac{w \ \sin(\beta')}{\sin(90° - \beta' - \gamma)}$$

therefore

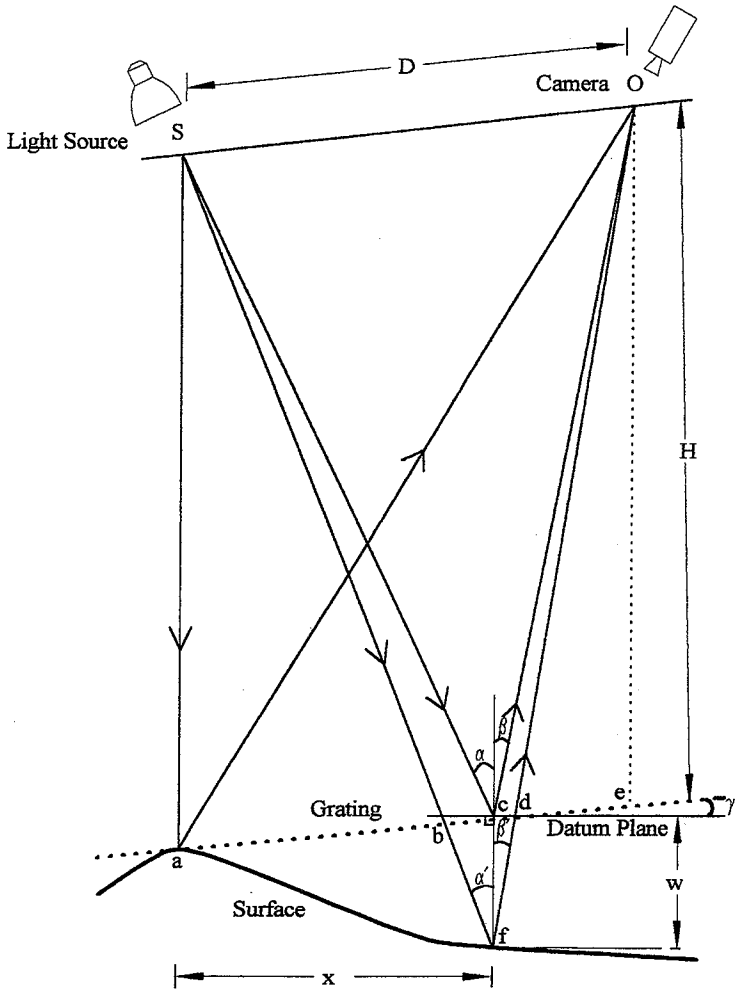

FIGURE 3 Typical shadow moiré system.

$$cd = \frac{w \sin(\beta')}{\cos(\beta' + \gamma)} \tag{6}$$

In Δbcf

$$cf = w \tag{7}$$

$$\angle cbf = 180° - \alpha' - (90° - \gamma)$$
$$= 90° - \alpha' + \gamma \tag{8}$$

$$\angle bfc = \alpha' \tag{9}$$

because

$$\frac{bc}{\sin(\angle bfc)} = \frac{cf}{\sin(\angle cbf)} \tag{10}$$

therefore

$$bc = \frac{cf \sin(\angle bfc)}{\sin(\angle cbf)}$$

Substituting equations (7) through (9) into equation (10)

$$bc = \frac{w \sin(\alpha')}{\sin(90° - \alpha' + \gamma)} \tag{11}$$

therefore

$$bc = \frac{w \sin(\alpha')}{\cos(\alpha' - \gamma)} \tag{12}$$

From Figure 3

$$bd = bc + cd \tag{13}$$

Substituting equations (6) and (12) into equation (13)

$$bd = \frac{w \sin(\alpha')}{\cos(\alpha' - \gamma)} + \frac{w \sin(\beta')}{\cos(\beta' + \gamma)}$$

$$bd = w\left[\frac{\sin(\alpha')}{\cos(\alpha' - \gamma)} + \frac{\sin(\beta')}{\cos(\beta' + \gamma)}\right] \tag{14}$$

From equations (1) and (14)

$$w\left[\frac{\sin(\alpha')}{\cos(\alpha' - \gamma)} + \frac{\sin(\beta')}{\cos(\beta' + \gamma)}\right] = Np \tag{15}$$

hence

$$w = \frac{Np}{\dfrac{1}{\cot(\alpha')\cos(\gamma) + \sin(\gamma)} + \dfrac{1}{\cot(\beta')\cos(\gamma) - \sin(\gamma)}} \tag{16}$$

Also, from Figure 3,

$$\cot(\alpha') = \frac{\dfrac{H}{\cos(\gamma)} + w}{x} = \frac{H + w\cos(\gamma)}{x\cos(\gamma)} \tag{17}$$

and

$$\cot(\beta') = \frac{\dfrac{H}{\cos(\gamma)} + w}{D\cos(\gamma) - x} = \frac{H + w\cos(\gamma)}{[D\cos^2(\gamma) - x]\cos(\gamma)} \tag{18}$$

Substituting equations (17) and (18) into equation (16) and simplifying yields

$$aw^2 + bw + c = 0 \tag{19}$$

in which

$$a = D - Np\cos^2\gamma$$
$$b = DH\cos\gamma - 2HNp\cos\gamma + NDp\sin\gamma\cos^2\gamma - Nxp\sin(2\gamma)$$
$$c = -Np[H^2 - HD\sin\gamma\cos\gamma + 2Hx\sin\gamma - xD\sin^2\gamma\cos\gamma + x^2\sin^2\gamma]$$

If the grating is not tilted (i.e., parallel to the plane of the surface), then γ=0°and equation (19) becomes

$$a_0 w_0^2 + b_0 w_0 + c_0 = 0 \tag{20}$$

where

$$a_0 = D - Np$$
$$b_0 = DH - 2HNp$$
$$c_0 = -NH^2 p$$

Solving equation (20), we obtain the two real roots of the quadratic equation

$$w_{01} = -H$$

and

$$w_{02} = \frac{Np}{\frac{D-Np}{H}}$$

Ignoring the first root, w_{01}, the surface height variation is

$$w = w_{02} = \frac{Np}{\frac{D-Np}{H}} \tag{21}$$

If the distance between the observer plane and the grating plane, H, is larger than the surface height variation, w (i.e., $H \gg w$), from the property of similar triangles $D \gg Np$. Hence, equation (21) may be simplified to yield

$$w = \frac{Np}{\frac{D}{H}} = N(p\frac{H}{D}) \tag{22}$$

Equation (20) is the equation for the geometric interpretation of the shadow moiré method with the setup shown in Figure 3, whereas equation (22) is the corresponding simplified equation so long as the distance between the observer plane and the grating plane, H, is much larger than the surface variation, w, and the grating plane is not tilted (*5*).

If the sensivity, namely, the contour interval Δh, is defined as

$$\Delta h = \frac{w}{N}$$

then from equation (22)

$$\Delta h = \frac{pH}{D} \tag{23}$$

Equation (23) indicates that the contour interval, or sensitivity, is related to only three parameters, which can be easily adjusted physically. Note from equation (22) that the surface variation, w, is obtained if N, the total number of fringes, or fringe order, is known. The contour interval $\Delta h = w/N = pH/D$ is the surface variation represented by each fringe. Equation (23) may be used with gratings whose tilt angle, γ, is smaller than 10° without producing appreciable error (*6*). Typically, such errors are smaller than 5 percent of the results obtained from equation (23).

SURFACE ELEVATION ERROR

To evaluate the accuracy of surface elevations measured by means of the shadow moiré method, an error analysis was conducted. In the error analysis, $z(x_i,y_j)$ represents actual surface elevation values and $z'(x_i,y_j)$ represents the computed elevation values derived from the shadow moiré method, where i=1, 2, 3,..., m and j=1, 2, 3,..., n. The planar coordinates x_i and y_j define the centerline locations of all fringes within a particular interferogram image. The difference between the actual and computed surface elevation values is denoted by

$$d_k = z(x_i,y_j) - z'(x_i,y_j) \qquad \text{where } k = 1, 2, 3,..., mn \tag{24}$$

Another set of elevation values, $z_k''(x_i,y_j)$, from which a third surface may be generated, may be obtained. Because nm difference values exist for d_k, nm sets of third surface elevation values, $z_k''(x_i,y_j)$, from which this third surface may be constructed, may be obtained. According to this, the error between the computed elevation values, $z'(x_i,y_j)$, and the actual surface elevation values, $z(x_i,y_j)$, is transferred to the error between the third surface elevation values, $z_k''(x_i,y_j)$, and the actual surface elevation values, $z(x_i,y_j)$. This error is denoted by

$$e = \min(e_k) \tag{25}$$

where

$$e_k = \sum_{i=1}^{m}\sum_{j=1}^{n} \frac{\left| z_k''(x_i,y_j) - z(x_i,y_j) \right|}{z(x_i,y_j)} \qquad \text{for } k = 1, 2, 3,..., nm \tag{26}$$

Extensive trials have shown that the shadow moiré method yields elevation values that are no more than 4 percent in error with respect to measured elevation values (*6*). Such trials involved a series of five parameter groups, in which each independent parameter varied and the error between computed and measured elevation values was determined.

INVESTIGATION

The prototype road inspection vehicle is a uni-axle enclosed trailer. The interior dimensions of the trailer conform to the distance requirements of D and H, which are functions of the contour interval Δh, as discussed previously. A user must initially select the desired sensitivity, or contour interval Δh. Based on this chosen value of Δh, the ratio of H/D must be satisfied in equation (23). Selection of the interior trailer dimensions is based on satisfying the H/D ratio. In the prototype road inspection vehicle, H/D was 3.3 for a chosen contour interval Δh of 6.6 mm (0.26 in.), which satisfies equation (23). This particular value of Δh allows detailed mapping of most roadways while reducing redundant fringe formation due to extreme sensitivity. The smallest useful value of Δh is approximately 3.2 mm (0.125 in.).

TRAILER FLOOR MODIFICATION

The wooden trailer floor was modified to accommodate a single large grating 180 cm (71 in.) in width, which allows a half lane of roadway to be mapped in a single pass. Modification of the trailer floor consisted of cutting a rectangular opening on the floor and adding steel beams to the two sides of the opening at the front and rear of the trailer. The steel beams, used to mount the grating to the opening, add rigidity to the trailer floor. The depth of the steel beams had to be considered, because two vertical sets of holes had to be drilled in each beam for placement of the grating. These sets of holes facilitate various configurations of mounting the grating and allow various grating tilt angles to be realized.

GRATING

A single large grating was constructed and mounted in the floor opening of the trailer. Approximately 450 strands cover the area of the trailer floor opening where the shadow moiré interference will occur. This area is approximately 180 cm (71 in.) by 81 cm (32 in.). Using a single grating instead of two smaller gratings eliminated the 15.24-cm (6-in.) grating frame obstruction at the center of the opening. This obstruction resulted in a loss of over 1310 cm^2 (203 in^2.) of road surface mapping area. Furthermore, the center obstruction created hard shadows on the road pavement, thereby producing null regions in the interferograms.

INTERNAL FRAMEWORK

The internal framework of the trailer is designed to fit over the grating opening. The frame serves as a mount for both the CCD video camera that captures the interferograms and the high-intensity lighting system. In addition, the frame adds overall stiffness to the trailer, because it is mounted both to the trailer=s walls and to its floor. The height of the frame is critical, because the vertical distance from the top of the frame to the grating is the H value in equation (23). Hence, the contour interval Δh is a function of both the height of the frame and the depth of the steel beams that support the grating.

LIGHTING SYSTEM

Extensive research and design went into creating a lighting system with the illumination and optical characteristics needed for the shadow moiré method. The lighting system comprises four white light, line-type condensing units, with a total output of approximately 4,200 W, mounted on top of the internal frame. Each unit uses a 50.8-mm (2-in.) quartz filament lamp, consuming 1,050 W of power. The coiled filaments, which are only 25.4 mm (1 in.) in length, are encapsulated in each lamp.

CCD VIDEO CAMERAS

To capture interferograms along the roadway, a CCD video camera is mounted in the trailer at the top of the internal frame and opposite the lighting system. This camera, which is directed at the grating, employs a fast 1/10,000-sec shutter speed to prevent blurring of the fringe patterns at highway speeds. The camera captures interferograms in a 256 grey scale, has a resolution of 512 × 480 pixels, and can be operated in two modes—frame and field. Field mode allows 60 images to be captured per second, compared with 30 images/second that can be captured with the frame mode. An image of the flashing light-emitting diode (LED) cluster mounted at the edge of the grating also is captured by the camera. The camera must be connected to an image freezer unit for it to operate. The image freezer, which supplies electricity to the camera, facilitates adjustment of shutter speed, as well as options such as digital image capture or image freezing. The actual freezing feature is not used because the frozen image deteriorates when it is stored in the low-resolution video memory of the image freezer.

A second CCD video camera, mounted approximately mid-height on the frame, provides a panoramic view of the interior of the trailer, allowing users in the towing vehicle to assess any trouble that might develop in the trailer during a highway field inspection. Both CCD video cameras are connected to a pair of display monitors mounted inside the towing vehicle.

VENTILATION SYSTEM

A ventilation system is installed on the roof of the trailer, directly over the lighting system, to prevent electrical components from overheating. Most electrical equipment inside of the trailer must be operated at temperatures below 40°C (104°F). The ventilation system consists of a 110-V alternating current (AC) fan and "top hat" to prevent stray light from entering the trailer.

ELECTRICITY GENERATOR

A gasoline-powered electricity generator inside the trailer powers all electrical components of the towing and road inspection vehicle, except for a pair of digital counters. An exhaust pipe attached to an opening on the trailer wall allows exhaust fumes to be released outside the road inspection vehicle. The generator uses a four-stroke, 11.94-kW (16-hp) Briggs and Stratton engine capable of producing 8 kW of continuous electrical power and has 110-V and 220-V AC output sockets. The generator can operate for more than 5 hours on one tank of fuel.

CONFIGURATION OF SUBSYSTEMS

The road inspection system is configured into three subsystems: video acquisition, distance measuring, and image processing.

Video Acquisition Subsystem

The video acquisition subsystem consists of a high-resolution CCD video camera, a video image freezer, a frame code generator, and a U-Matic videocassette recorder (VCR). The subsystem continuously records all fringe patterns within the grating area and issues a frame code to each frame recorded by the VCR.

Video Image Freezer

The video image freezer facilitates control of a single CCD video camera. The image freezer can set various functions, such as shutter speed, vertical synchronization, and video image storage. The video image freezer is connected to the CCD video camera, which captures the interferograms within the grating area.

Frame Code Generator

The frame code generator issues sequentially numbered frame codes that are recorded simultaneously with the video images onto the videotape. Each frame along the videotape must be numbered so that it can be found during postprocessing. The frame code generator, which is located in the towing vehicle, generates 6-digit frame codes and inserts them between 17 Hz and 18 Hz of the vertical blanking of the video signal. Frame codes are generated from 000000 to 299999 and correspond to 2 hr 46 min when timed with a National Television Standards Committee (NTSC) signal. The code returns to 000000 when it exceeds 299999.

Frame code insertion can begin in one of the following ways, in accordance with the START TRIGGER switch setting on the front panel:

- External pulse—The unit begins code insertion when an external pulse is detected after the START button is depressed.
- Cue tone—The unit begins to insert codes when a 1-kHz cue tone is detected after the START button is depressed.
- Manual—The unit starts code insertion when the START button is depressed.

U-Matic VCR

The VCR used to store image data, an industrial-quality U-Matic VCR, provides 500 lines of resolution with a signal-to-noise ratio better than 48 dB. The U-Matic is a single, rack-mountable VCR with all controls on the front panel. In addition to all the outstanding features of conventional VCRs, such as production of a high-quality picture, simple remote control, picture search, and programmed operation, this VCR features frame code addressing. It records onto high-resolution 1.904-cm (0.75-in.) videotape. Each videotape is approximately 75 min in duration, allowing for a maximum of 108 km (67.5 mi) of roadway to be inspected continuously. The VCR is located in the towing vehicle to record fringe pattern images. In the postprocessing facility, a videocassette player (VCP) is used to play back the videotape so that it can be processed and analyzed.

Distance Measuring Subsystem

The distance measuring subsystem accomplishes two important tasks: keeping track of the distance traveled by the road inspection vehicle and flagging fields along the videotape pertaining to covered mapping intervals. As the road inspection vehicle travels along the road, incremental image mapping of the road surface takes place in a sequential manner to avoid gaps and overlapping. Because the VCR in the towing vehicle records continuously, certain flags must be placed along the videotape to indicate which fields pertain to mapping intervals. This is required because the vehicle is unlikely to travel at a constant speed.

The flagging technique used in the road inspection vehicle (*7*) employs two high-luminosity LEDs that flash in a predetermined sequence at every mapping interval. Because the LEDs are mounted at the edge of the grating, the video camera captures both the LED flashes and the corresponding fringe pattern within the grating area. Two Gemini 1000 digital pulse counters are fed distance data by means of the van's electronic speed sensor. The counters trigger each LED to emit a flash. The counters do not display distances traveled, but they do display the number of pulses emitted by the speed sensor.

When playing back the videotape during postprocessing, only fields pertaining to specified mapping intervals are analyzed. A special image processing algorithm was written to allow only fields containing the correct LED flash sequence to be analyzed. By summing the number of LED flashes from a starting point, the location of a particular surface distress can be determined accurately from the videotape.

The surveyor counter, a programmable multifunction digital counter, is similar to the two Gemini 1000 counters, in that it uses the pulse stream of the van's speed sensor and is capable of displaying the distance traveled by the vehicle, vehicle velocity, and other parameters in specified units. The surveyor counter, programmed to display feet traveled by the road inspection vehicle, is mounted inside the van and provides accurate distance tracking.

Image Processing Subsystem

The image processing subsystem, which is dedicated to postanalysis of the videotape, consists of an image processor, various specialty modules housed in the image processor, VCP, a VCP-computer interface board, and a 100-MHz Pentium personal computer. During postanalysis, the videotape is played back field by field, and only fields displaying the correct LED flash sequence are processed. The image processing algorithms, written to analyze digitized fringe pattern images, are used to rate and extract three-dimensional contour data. Several image processing algorithms, developed to accomplish a multitude of image postanalysis tasks, are written in the C programming language and are fully integrated into a user-friendly master program.

Image Processor

The image processor, a stand-alone unit that processes images in real time, is capable of performing image-intensive functions such as image averaging, image subtraction, convolution, edge enhancement, binarization, and histogram operations. The image processor has an AT-to-VME video bus that interfaces with the PC. The bus is a high-speed, dedicated bus that transfers image data between image processing modules without burdening the host computer.

A video source, such as a camera or VCR, produces an analog video signal that contains image data. The signal is transmitted to the image processor and converted to digital picture elements or pixels. The digital pixel data are stored in frame memory one field at a time, with each pixel occupying a single frame memory location. Once the image has been stored in frame memory, it may be accessed for additional processing. Display circuitry transforms the pixels stored in frame memory back into an analog signal for display on a video monitor. The base configuration includes a seven-slot chassis, host computer interface, analog/digital module, frame buffer, and pipeline processor. This high-speed image processor can perform 10 million operations per second.

Analog/Digital Module. The analog/digital module interfaces with standard (RS-170, -330, CCIR) video sensors and monitors. This module supplies data and synchronization to other modules. It features an 8-bit or 256 gray-scale

digitizer, programmable gain and level, a full complement of input and output look-up tables, and pseudocolor or 24-bit true color display.

Frame Buffer. The frame buffer contains enough frame memory for all of the image storage typically required in a basic image processor configuration. Image storage does not occupy central processing unit memory. Frame memory is accessible to the CPU and all other modules. Each frame buffer contains a 16-bit frame store and two 8-bit frame stores with 512 × 512 resolution. The 16-bit frame store serves as an accumulator to hold processed images where intermediate results are greater than 8 bits. Frame summation and convolutions are typical of these types of image processing operations. The frame buffer features unique advanced frame memory architecture that provides the flexibility and power required in high-performance image processing subsystems. Up to four frame buffers can be used for increased on-line image storage. The increase in the availability of frame stores, which allows rapid random accessing of image data by the host computer, permits the analysis of generalized fringe patterns to take place in a reasonable length of time.

Pipeline Processor. The pipeline processor is a high-performance processor providing real-time arithmetic, logical, and bit-plane-oriented image processing capabilities. The processor's advanced architecture allows it to perform many common image processing functions while maintaining 16-bit accuracy throughout the processing pipeline.

The pipeline processor consists of the following:

- Switching—The cross-port switch at the input of the module allows selection of a variety of sources for video input.
- Multiplication—Pixels are multiplied by a constant, or two 8-bit pixels are multiplied to form a 16-bit resultant.
- ALU—Two 16-bit operands are combined either arithmetically or logically.

Pipeline processor functions include addition, subtraction, AND, OR, and XOR with masking. In addition, the pipeline processor contains the following complex functions:

- Barrel shifter—Performs arithmetic and logic (rotate) shifts on either unsigned or complement data for scaling and shifting.
- Clipper—When enabled, the clipper takes the absolute value of the result of the barrel shifter.
- Byte-swap—Conditionally controlled, the byte-swap mechanism allows the output data path of the processed pixels to be selected.
- Output lookup tables (LUTs) —Two sets of eight programmable LUTs (256 × 8 bits each) perform point processing on the resultant pixels before storage or additional processing.

Videocassette Player

The VCP used for postprocessing is identical to the VCR in the towing vehicle, except that it does not have recording capabilities. Frame codes can be extracted from the VCP.

VCP-Computer Interface Board

To control the VCP by computer, an interface card is installed between the VCP and the host computer. This interface board reads the frame code equivalent for the absolute address, communicates with the external computer by the RS-232 protocol, and organizes the interactive video system. The factory-preset communication protocol data format follows:

- Mode: asynchronous,
- Character length: 8 bits,
- Baud rate: 9600 bps,
- Parity check: none,
- Stop bit: 1 bit.

Only the baud rate is variable. Also, several switches are available.

Baud Rate Switch. Available baud rates are 9600, 4800, 2400, and 1200 bits/sec. The baud rate switch of the interface board is set to match the baud rate of the external computer before the power is turned on.

Video/Audio Mute Clear Switch. When this switch is off, the video and audio outputs are muted while a frame code is being searched. When this switch is on, a picture is displayed on the screen while a frame code is being searched, the muting of the video and audio outputs is cleared, and the audio signal is available.

Fast Forward/Rewind Clear Switch. When this switch is off, a designated frame code is searched at a high speed using the fast forward and rewind modes. When this switch is on, the unit searches for and reads the frame code without being in the fast forward and rewind modes.

Operation Selection Switch. In the off position, the frame code is read automatically. When it is on, the frame code is not read. This switch operates only when a cassette is inserted.

Remote to Local Switch. In the off position, when the host computer is on, all function keys at the VCP side except EJECT are disabled. When on, all keys on the VCP are operational, and the VCP can be controlled by the computer.

Host Computer

A Compaq DeskPro XL 5100 PC is used during postprocessing. This computer features a 100-MHz Pentium processor, PCI bus, 16-MB RAM, a 1.05-GB hard drive, and a single floppy drive. The PC is linked to the VCP by means of the VCP-computer interface board installed in the VCP. Communication between the computer and VCP is accomplished through a serial connection. The image processor bus interface, installed in one of the computer's internal slots, provides communication with the image processor.

RESULTS OF FIELD TESTING

The purpose of this research was to test the prototype road inspection vehicle in the field. Such testing was conducted over various pavement types and at different speeds to assess the performance of the entire system as well as each of its components. Several components required improvements based on the field test results. These improvements are described below.

Initial Performance of Components

Two Small Gratings

Originally, two small gratings were placed in the floor opening (Figure 4) of the trailer and tested in the field. Each grating was 81 cm × 81 cm (32 in. × 32 in.) and mounted within the steel frame. The quality of the interferograms produced by this configuration was very good. By placing two square gratings side by side, a rectangular combined grating area is created. At the center of this rectangular area was a 1310-cm^2 (203-$in.^2$) obstruction resulting from placement of the grating frames side by side. During field testing, the center part of the grating frame created several hard shadows along the road surface below the gratings. The number of hard shadows corresponded to the number of lighting units used during the field test. This is a consequence of using multiple lighting units, because they cannot be placed exactly at the center of the floor opening, above the gratings. The double grating configuration was therefore abandoned in favor of a single rectangular grating and frame.

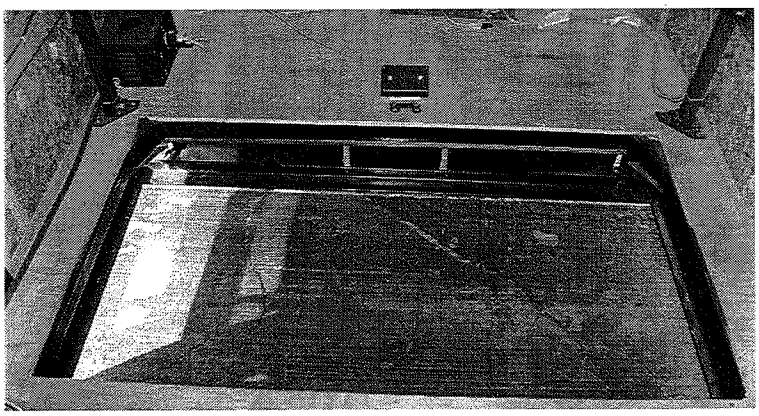

FIGURE 4 Trailer floor opening.

Lighting Units

Four high-power, quartz filament lighting units were used to illuminate the gratings so that interferograms could be produced (Figure 5). Each lighting unit consisted of a 1,000-W filament and reflector. All four lights were mounted side by side along a 180-cm (71-in.) steel mount. On the front of the mount, two long aluminum plates were affixed, each spanning 180 cm. By adjusting the distance between the plates, a slit could be created. This slit allows a narrow horizontal band of light to be projected onto the gratings. The shadow moiré technique requires that the light emitted from a line source be parallel to the strands of the grating. Field testing of this lighting configuration resulted in the discovery that the projected light was not uniform in intensity across the width of the grating.

This anomaly in the light distribution resulted in poor binarization of the interferograms, thereby creating a loss of surface distress data. The slit configuration of the lighting units was discarded in favor of line-type condenser lenses with individual slits for each lighting unit. This new configuration resulted in the formation of a much more uniform light distribution on the grating, allowing for proper binarization of the interferograms.

Distance Tracking

The original distance tracking subsystem was a mechanical system consisting of several pulleys and a V-belt. A large pulley was attached to the wheel of the trailer. As the trailer moved, this large pulley rotated a smaller pulley attached to a shaft by means of a V-belt. The shaft was mounted above the wheel and through the trailer wall. A transparent circular disk and infrared sensor were placed at the end of the shaft. This configuration resulted in rotation of the disk in response to the movement of the trailer. The infrared sensor was placed perpendicular to the transparent disk. A black notch was fixed to the transparent disk to trigger the sensor. This setup triggered the sensor when the trailer traveled the distance equivalent to one mapping interval. The sensor flashed a single LED on the LED cluster located at the edge of the trailer floor opening. Field test results (Table 1) demonstrate that this configuration was accurate at speeds below 15 km/hr.

At higher speeds, however, the accuracy of this configuration dramatically decreased, with errors approaching 8 percent. The main problem was skipping of the V-belt due to the vertical displacement of the wheel over severely distressed roadways. This method of distance tracking was abandoned in favor of a completely electronic approach using the towing vehicle's built-in speed sensor.

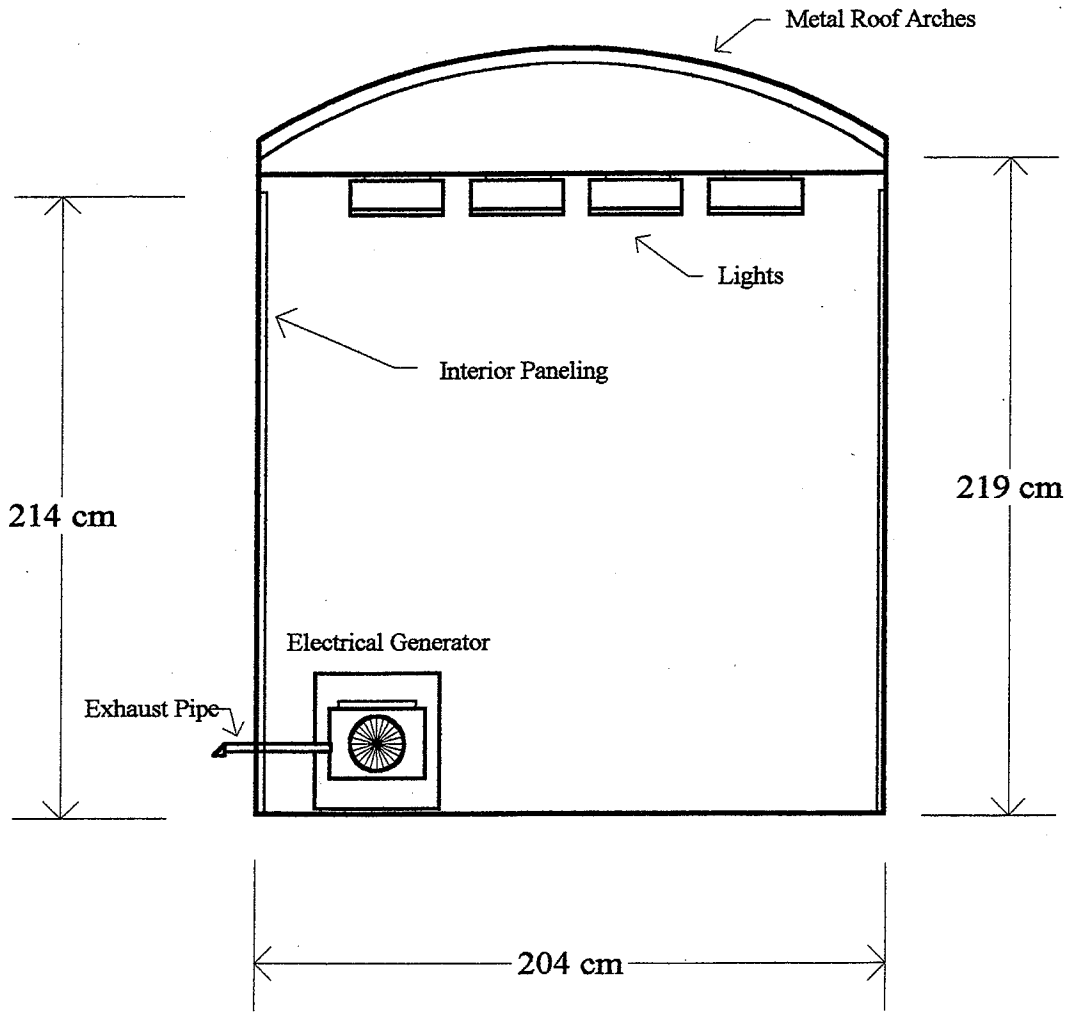

FIGURE 5 Placement of lights in the road inspection vehicle.

TABLE 1 Results from Field Testing of Mechanical Distance Tracking Subsystem

Measured Distance (m)	Calculated Distance (m)	Difference in Distances (%)	No. of LED Flashes	No. of Mapping Intervals
112.69	112.68	-0.01	143	142
139.68	139.66	-0.02	177	176
184.86	184.89	0.02	234	233
185.53	185.50	-0.02	235	234
194.39	194.41	0.01	246	245
276.04	276.05	0.01	349	348
300.47	300.45	-0.01	380	379
305.43	305.49	0.02	386	385

Magnetic-Inductance Sensor Approach

Originally, much effort and time went into developing a distance measuring subsystem capable of producing approximately 70,200 pulses/km (113,000 pulses/mi). This subsystem was designed around a 150-tooth steel sprocket, which was mounted on the trailer's drum brake assembly. As the trailer wheels rotated, the sprocket rotated. A magnetic-inductance sensor was then secured to the nonrotating backing plate of the drum brake, thus allowing the sensor to count each tooth of the sprocket. Both the sensor and sprocket were mounted to take advantage of the trailer's suspension, thereby producing a fixed distance between them and eliminating the possibility of displacement on severely distressed roadways. Figure 6 shows the sprocket mounted on the trailer's drum assembly.

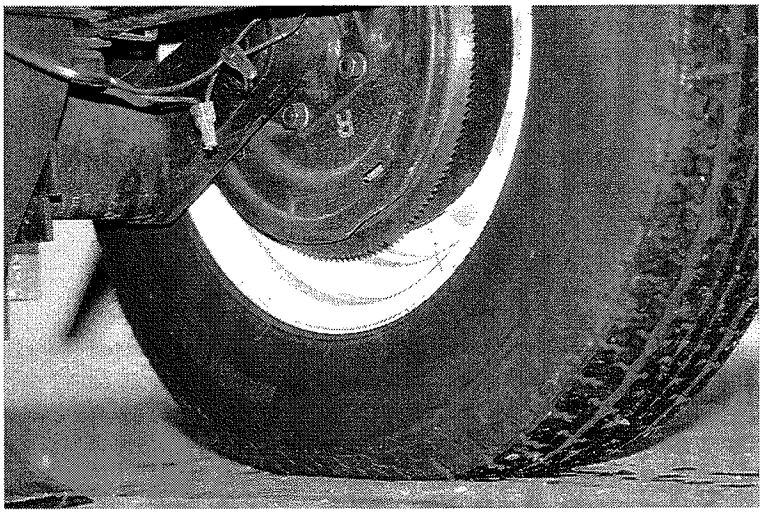

FIGURE 6 The Gemini 100 digital pulse counter, the sensor, and the steel sprocket.

Preliminary testing of this configuration in the laboratory yielded excellent results. A Gemini 1000 digital pulse counter displayed the number of pulses emitted by the sensor and flashed an LED after a predetermined number of pulses were detected. By measuring the number of pulses per unit distance, a constant was determined and programmed into the counter. This constant was on the order of 4.53 cm/pulse (1.81 in./ pulse.) Because the width of the grating was 77.72 cm (31.6 in.), 77.72/4.53, or approximately 17 pulses, had to be detected by the counter to produce a single LED flash. The idea was to obtain an LED flash when the vehicle traveled a distance equal to the grating width. This resulted in perfect mapping of the roadway, because only fields along the videotape displaying an LED flash were processed.

Field testing of this configuration, however, yielded poor results. A significant investigation was initiated to determine the cause. This investigation showed that the gasoline-powered electricity generator caused the trailer's frame to vibrate at a high frequency. The vibrations could not be detected by the naked eye, but could be detected by touching any component of the trailer's frame. Further investigation showed that the magnetic-inductance sensor was affected by even minute vibrations. The sensor not only detected ferrous objects (steel sprocket teeth), but also the magnetic field created when the magnet in the tip of the sensor came close to the teeth of the sprocket. The vibrations created a flux in the magnetic field, thereby triggering the sensor to send a pulse to the digital pulse counter.

Dampening the generator's mounting hardware was deemed futile, because any severe road distress will cause vibrations to be propagated throughout the trailer's frame. Hence, the magnetic-inductance sensor approach for distance tracking was abandoned. Other sensors were considered, but each had its own limitations, such as inadequate maximum count rates in optical encoder sensors, extremely low sensor-to-sprocket distance requirements, and various vibration problems similar to those encountered with magnetic-inductance sensors.

LED Cluster

The original LED cluster consisted of a 9.525-mm (3/8-in.), high-luminosity LED. The cluster, located at the edge of the trailer floor opening, was videotaped along with the corresponding inteferograms occurring within the grating areas. Maximum usable vehicle speed for surface distress data acquisition was approximately 72 km/hr (45 mi/hr), which is based on both LED flash duration and NTSC video synchronization timing. During postanalysis, the videotape was played back field by field. Only fields pertaining to LED flashes were analyzed by the image processing subsystem. By summing the number of LED flashes from a starting point, the distance traveled by the road inspection vehicle corresponding to each interferogram was determined easily.

Field testing confirmed that the single LED was an accurate way to separate mapping intervals and distance tracking. Further improvement of this technique led to a twin LED cluster.

Refinements and Improvements

All road inspection system components were modified or improved based on field test results. A discussion of updated components and their performance in the field follows.

Single Large Grating

Much research went into developing a single large rectangular grating to remedy the problems of mapping area loss and hard shadow creation (Figure 7). The frame of the new grating was constructed from lightweight aluminum, for ease of mounting within the confines of the trailer floor opening. Several field tests using polyester strands in the new grating resulted in vibration of the strands near the center of the grating at vehicle speeds exceeding 40 km/hr (25 mi/hr) and in slower runs over severely distressed roads. These vibrations effectively "washed out" the interferogram, resulting in loss of road surface data. The polyester strands were replaced with steel strands. Because steel strands have a much higher modulus of elasticity than polyester strands, they are less prone to side-to-side vibration. The large grating frame is being modified to accommodate the steel strands. No field test results of the modified grating are available at this time.

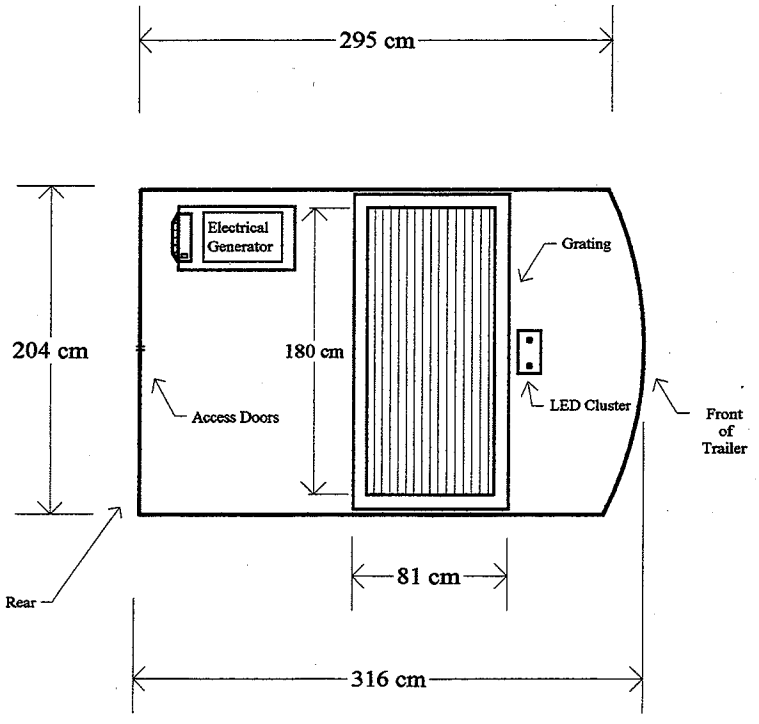

FIGURE 7 Single large grating in the floor of the road inspection vehicle.

Enhanced Lighting Units with Condenser Lenses

The most crucial aspect of designing new lighting units was to create the proper line source condenser lens for each unit. These lenses had to maximize the efficiency of the light produced from the quartz filament lamps, while acting as

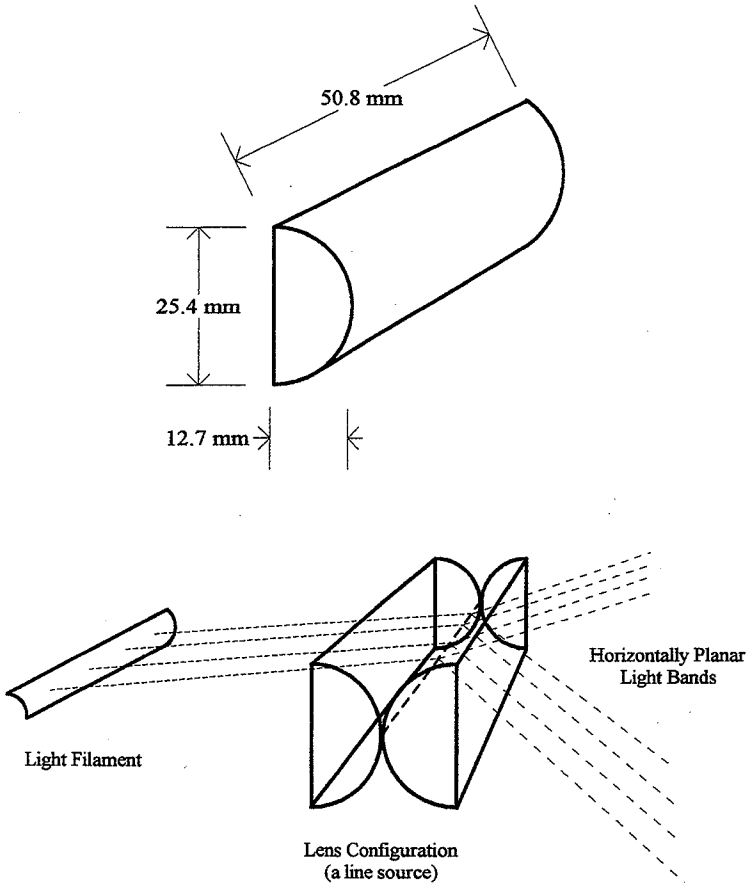

FIGURE 8 Enhanced lighting unit with condenser lenses.

a horizontal line source. A horizontal line source is a line in which all light rays propagate away from the line normally. To create such a line, two half-cylinder lenses must be mounted back to back so that their only contact is a line that runs the length of each half-cylinder lens. Each lens has a 12.7-mm (0.5-in.) radius and a length of 50.8 mm (2 in.). Figure 8 illustrates the lighting unit.

Extensive field testing revealed that the new lighting units produced a much more uniform illumination plane compared with lighting units without condenser lenses. Uniform illumination is mandatory for proper binarization of interferograms. Observation and analysis of interferograms produced by the new lighting units revealed a dramatic improvement in fringe-to-background contrast. This improvement is the result of using a near-ideal line source lighting system, in which the line source light wave propagation pattern is parallel to the strands of the grating. Further field testing revealed that the best possible lighting configuration for the shadow moiré method is one in which a single lighting unit, along with its two condenser lenses, is used to create the interferogram. Testing of a single 1,050-W lighting unit with condenser lens yielded the cleanest and sharpest interferograms and the best interferograms over dark asphalt pavement. High illumination is needed to produce an interferogram bright enough to be used with dark asphalt pavements. It was concluded that the ideal lighting system for both dark and light pavements is a single-filament unit with two condenser lenses and a power consumption in the range of 3,000 to 3,500 W.

Improved Distance Tracking

The improved distance measuring subsystem uses a pulse stream signal generated by a speed sensor in the towing vehicle's transmission. Such speed sensors are common in late-model ABS-equipped vehicles. The speed sensor produces approximately 4,970 pulses/km (8,000 pulses/mi); each pulse is at +5-V high and under +1-V low. Two Gemini 1000 programmable digital pulse counters are connected to the pulse stream to tally the number of pulses emitted by the speed sensor. Each counter is connected to its own high-luminosity LED. When the counters receive a

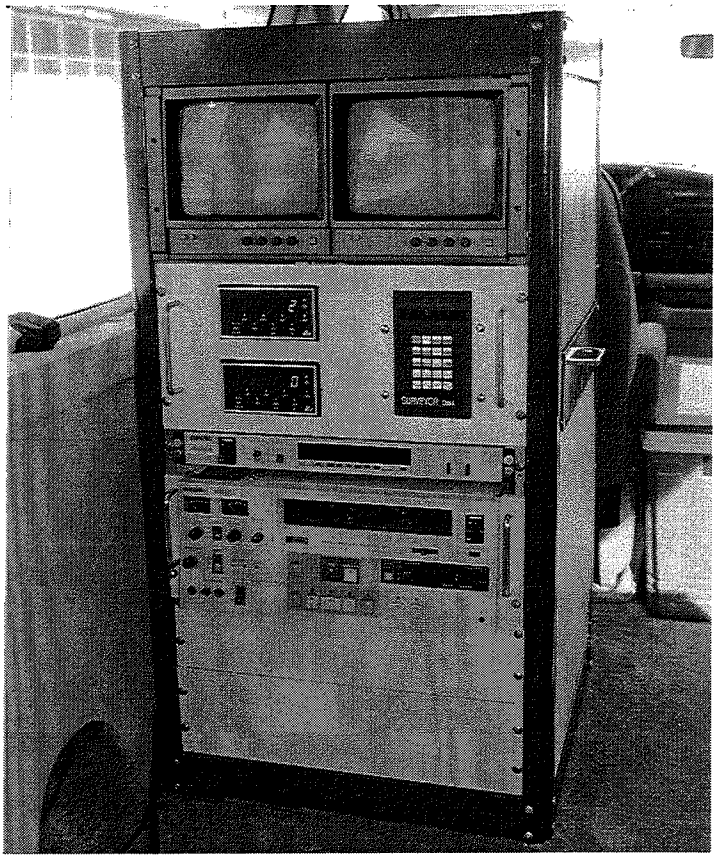

FIGURE 9 Gemini 1000 digital pulse counters and other equipment in the van.

certain number of pulses sent by the speed sensor, they flash their corresponding LED. Each counter is programmed to flash its LED at different pulse counts, thereby producing a unique LED flashing sequence. A flash from either LED corresponds to a distance equivalent to a mapping interval traveled. Both counters are housed inside the van (Figure 9).

Field test results of this new configuration yielded consistent distance tracking data, primarily because of the elimination of the mechanical defects noted in the previous subsystem design. Tests conducted over severely distressed roadways at near-highway speeds also produced consistent distance tracking data. Accuracy of this improved subsystem is slightly higher than the mechanical distance tracking subsystem, with an average random error of only 0.0125 percent between measured and actual distances traveled. Table 2 presents results from the initial field testing of the improved distance measuring subsystem.

TABLE 2 Results from Field Testing of Electronic Distance Measuring Subsystem

Measured Distance (m)	Calculated Distance (m)	Difference in Distances (%)	No. of LED Flashes	No. of Mapping Intervals
1085.52	1085.65	0.01	1369	1368
1073.88	1073.75	-0.01	1354	1353
697.51	697.57	0.01	880	879

Dual LED Cluster

A new LED cluster was constructed to house two high-luminosity LEDs. Each LED is connected to a Gemini 1000 programmable digital pulse counter, which in turn is connected to the pulse output of the vehicle's speed sensor (Figure 10). Because the pulses emitted by the speed sensor are constant, an increase in data acquisition speed of 22 percent has been realized by using two LEDs instead of one. The previous mechanical distance measuring subsystem consisted of a single LED and an infrared sensor whose pulse duration was a function of vehicle speed. The new subsystem can track the distance traveled by the road inspection vehicle at speeds up to 88 km/hr (55 mi/hr) compared with the original subsystem=s maximum speed of 72 km/hr (45 mi/hr.)

The constant pulse of the vehicle's speed sensor ensures that no more than two fields along the videotape capture a single LED flash. Field test results at 86 km/hr (53 mi/hr) confirm that only one or two fields along the videotape capture an LED flash along with a separation field, which contains no LED flash. Separation fields are important because they function as terminators of individual LED flashes. Vehicle speeds beyond 88 km/hr (55 mi/hr) would force some LED flashes into separation fields, thereby resulting in incorrect LED flash counts by the LED track algorithm during postanalysis of the videotape.

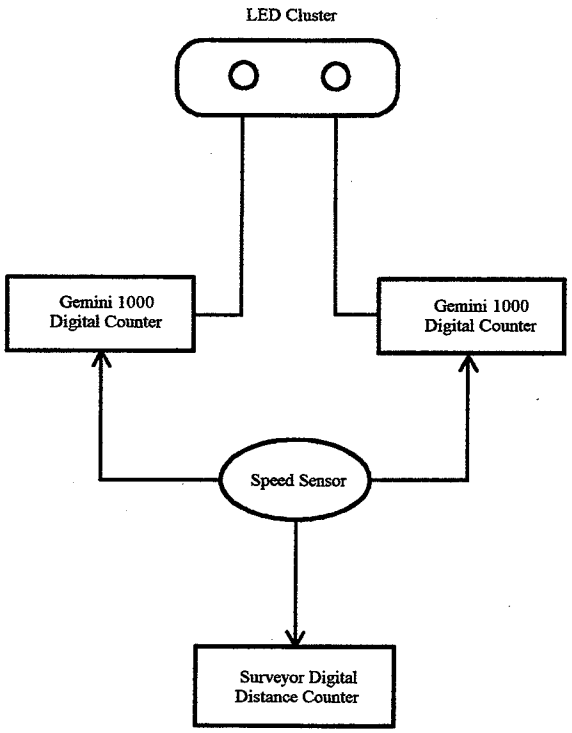

FIGURE 10 LED cluster's relationship in distance measuring subsystem.

Video Acquisition Card Approach

A Data Translation DT-3155 video acquisition card was installed inside the Pentium host computer. Although this card is not required for postanalysis, it is being evaluated as an alternative to the image processor and possibly to the VCR and VCP. The possible uses of the DT-3155 are twofold. First, it could be used to digitize interferograms previously recorded onto videotape. Sending digitized images from the image processor to the computer for processing requires that the information flow through several serial port bottlenecks, thus increasing the time for performing postanalysis. Because the DT-3155 is installed in the host computer, digitization of interferograms occurs directly in the computer's CPU. Once the digitized images are in the host computer's RAM, fast post-analysis can be accomplished by the computer's 100-MHz Pentium CPU instead of the slower 10-MHz image processor.

The second possible use of the DT-3155 is for real-time field image acquisition. The DT-3155 can be triggered by a Gemini 1000 digital pulse counter to capture the video output from a CCD video camera. The captured images could be stored on a removable hard disk drive in the van. This would require that a host computer be installed in the van. Once a field run has been completed, the operator would bring the removable hard disk drive to the postanalysis facility. At the facility, the removable hard disk drive would be inserted into another host computer for image analysis. All images captured on the removable hard disk drive would be ordered sequentially. Each image would be automatically binarized during acquisition, thus eliminating the need to run a separate binarization algorithm. This would result in vastly improved efficiency of postanalysis. Each image would require approximately 31.5 K on the removable hard disk drive. This method of video acquisition would eliminate the need for a frame code generator, VCR, VCP, and the LED cluster.

Image Processing Algorithms and Software

The image processing subsystem is composed of both hardware and software (Figure 11). A discussion of the software portion of the image processing subsystem follows.

LED Tracking Algorithm

The LED tracking algorithm uses the image processor to determine when LEDs flash during videotape playback in the postprocessing phase. This algorithm scans two square, predefined sections on the image pertaining to the location of each LED. By comparing pixel intensity values of each section, the algorithm can determine whether an LED emitted a flash. Fields containing an LED flash are considered flagged by the algorithm. Because two fields along a videotape may capture a single LED flash, the algorithm may interpret this situation as two LED flashes. To avoid this conflict, the digital pulse counters used in the towing vehicle are programmed to flash the LEDs in a predetermined alternating sequence. The algorithm has been designed to anticipate this sequence and keeps track of which fields along a videotape pertain to selected mapping intervals. The algorithm also keeps track of the distance traveled by the road inspection vehicle for every field containing an LED flash.

Postanalysis of videotaped field trials verified that the LED tracking algorithm is an accurate way to count LED flashes. The algorithm consistently chose fields along the videotape that contained valid increments of the mapping interval.

Screening Algorithm

The screening algorithm rates every flagged field on the videotape containing an LED flash on the basis of the severity of surface distress encountered. Two subroutines in this algorithm measure the amount of surface distress in each flagged field. The roughness (RH) subroutine determines the amount of vertical deformation encountered over a span of pavement. This subroutine counts the number of fringes in each flagged field to determine the out-of-plane deformation of the surface distress. The second subroutine determines the change-of-slope index (CSI), the amount of change in the slope of all fringes of a flagged field. The CSI, whose limits are 0.0000 and 1.0000, is a measure of the roughness of the surface distress. A flat surface would yield a CSI close to zero. Surfaces that contain various amounts of out-of-plane surface distress would increase the CSI. The maximum upper limit of CSI is 1.0000, which holds true if all fringes in a flagged field contain a slope of at least 45 degrees to the horizontal. The user of the road inspection system decides how the subroutine defines the maximum upper limit on the basis of specific requirements.

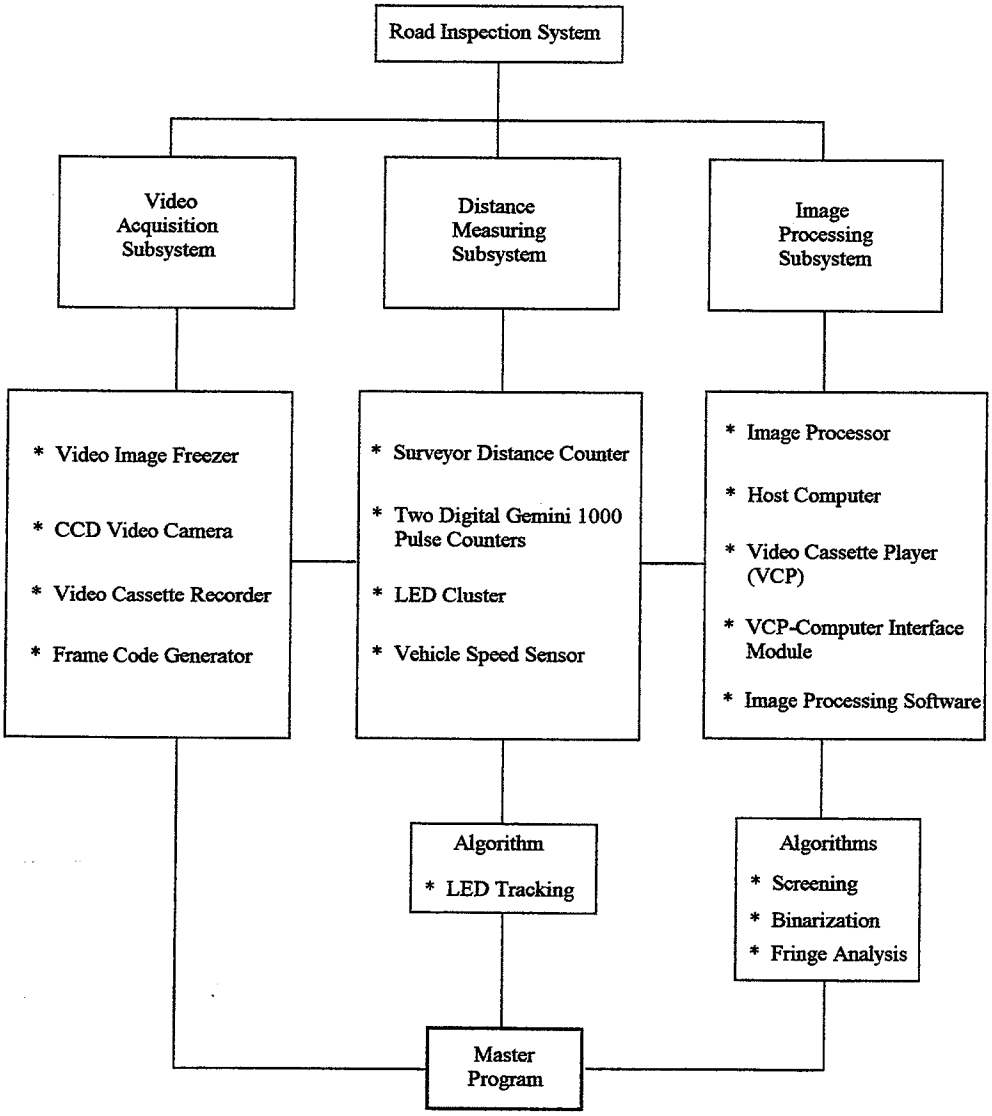

FIGURE 11 Three integrated subsystems.

The screening algorithm writes an ASCII file to the computer's hard drive during postprocessing. The ASCII file contains the distance traveled by the road inspection vehicle for each flagged field, the maximum vertical surface height deviation, the roughness value, the CSI, and the frame code along the videotape pertaining to the location of the particular field. Further analysis, such as three-dimensional surface reconstruction (*8*) of a specific field, requires entering the frame code into the computer, thus allowing the VCP to retrieve the field along the videotape. This procedure eliminates the need to save every flagged field as a graphics file in the computer's hard drive. Table 3 contains the results obtained from comprehensive field testing of this algorithm.

TABLE 3 Effectiveness of Screening Algorithm with Various Types of Distress

Type of Surface Distress	System Performance Relative to Type of Surface Distress (SD)	Performance of Roughness (RH) Subroutine	Performance of Change-of-Slope Index (CSI) Subroutine
Sagging and Rutting	5	5	5
Bumps	5	5	5
Washboarding	5	5	5
Out-of-plane cracks	5	5	5
Potholes			
with smooth curvature	4	5	5
with semicontinuous curvature	3	4	4
with discontinuous curvature	2	3	2
In-plane cracks	1	1	1

Note: 5 = excellent; 4 = very good; 3 = good; 2 = fair; 1 = poor.

The RH and CSI subroutines performed similarly, which indicates the heavy reliance of each subroutine on the shadow moiré indication of surface anomalies. Although performance of these subroutines is similar, they differ for surface distresses involving potholes caused by pavement dislodging. Pavement dislodging usually creates a steep drop, or depression, in the pavement. The RH subroutine, which is sensitive to vertical deformation along a surface, is better suited to detecting such distresses than the CSI, which analyzes changes in the horizontal slope of the pavement.

The following nonlinear relationships are indicators of subroutine performance for various types of surface distresses. These relationships, obtained by fitting the field test data, use a least-squares goodness-of-fit criterion.

$$RH = 3.39 + 0.063SD^3 - 0.041e^{SD} - \frac{2.34}{SD^2} \tag{27}$$

and

$$CSI = 68.96 - 4.45SD - 121.7\frac{\ln(SD)}{SD} - \frac{63.51}{SD^2} \tag{28}$$

where SD refers to system performance relative to a specific type of surface distress, as is defined in Table 3.

In an effort to correlate the surface distress elevation data obtained from the road inspection vehicle with pavement assessment values used by various state departments of transportation, it was found that roughness, an important indicator of pavement condition, can be determined easily and accurately by the shadow moiré system. In addition, the shadow moiré system can eliminate most difficulties in acquiring road surface data, while minimizing errors that appear to be inherent in other techniques. Road roughness is one of the major determinants of ride quality. Although the International Roughness Index (IRI) is widely used to quantify roughness and pavement quality, a similar index, IM_r, is used in North America. The IRI may be used to determine a pavement serviceability index (*9*). Roughness is defined mathematically as the total accumulative vertical deviation over the length of a test section. The units of measure used

for roughness are inches and miles, although units of meters and kilometers also may be used. As currently defined, roughness has no upper limit and its minimum value is zero for a flat surface.

For roughness to be computed, a positive deviation or elevation value must be defined. There are two traditional methods for defining roughness using elevation deviation values. One is the mean-square-average (MSA) and the other is the square-root-average (SRA). Referring to Figure 12, we define Δ_i as the elevation at point i. The MSA is defined mathematically as Δ_i^2; while the SRA is defined mathematically as $\sqrt{\Delta_i^2}$.

Roughness usually is defined as:

$$\frac{\sum_{i=1}^{j} \sqrt{\Delta i^2}}{L}$$

where i=1, 2,..., j (the number of data acquisition intervals).

Roughness measures in the transportation sector currently are obtained from three categories: (*a*) a profile numeric defined directly by a mathematical function from the absolute profile of road surface elevation; (*b*) summary numerics measured by a response-type system calibrated to a specific profile or other numeric by correlation; and (*c*) subjective rating of riding quality or pavement serviceability, usually made by a panel of raters within a scale defined by a subjective description (*10*). Differences and errors arise in all three categories because of the way the measuring instrument responds to the road profile and the way the data are processed. Difficulties inherent in current inspection systems make inaccuracies unavoidable because the acquired elevation values along the road surface are functions not only of surface distress, but also of other factors such as

- Vehicle speed,
- Dynamic response,
- Suspension dampening characteristics of inspection vehicle,
- Mass of vehicle and equipment, and
- Type of pavement.

A quarter-car simulation normally is used to analyze acquired elevation data (*11*). The preceding factors are considered in the simulation in an attempt to find the true roughness of the road.

The shadow moiré method keeps track of the number of fringes occurring in the grating for every mapping interval traveled. By allowing the road inspection system to count the number of fringes per image, the absolute value of

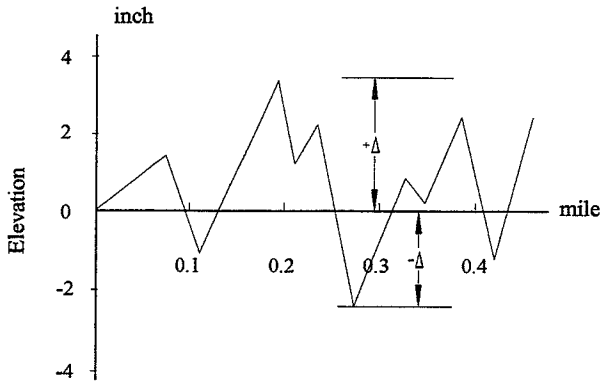

FIGURE 12 Roughness definition using elevation deviation values.

elevation is automatically obtained for each mapping interval. Each fringe represents one contour interval of vertical deviation. This method does not measure the vertical deviation between the grating and the road pavement; instead it measures the relative vertical deviation with respect to surface distress. The maximum error that can occur if the inspection vehicle skips or hops is $\pm \Delta h$. Such an error is not a function of the dynamic effects created by the suspension of the inspection vehicle; hence, it is unnecessary to run a quarter-car simulation with this method. The distance, L, traveled by the inspection vehicle is obtained by using the speed sensor in the vehicle. Roughness, based on the shadow moiré method, is defined as

$$\text{Roughness (in./mi)} = \frac{\sum_{i=1}^{j} (n-n_p)\Delta h}{L} \tag{29}$$

where

i, j = the number of mapping intervals;
n = number of fringes in the frame image;
n_p = $z/\Delta h$, the number of fringes corresponding to the tilt of the grating (for flat gratings, $n_p = 0$);
$\Delta h = pH/D$, a single contour interval expressed in inches; and
L = length of a roadway traveled by vehicle in miles.

Because $n_p = z/\Delta h$, equation (29) may be rewritten as

$$\frac{\sum_{i=1}^{j} (n\Delta h - z)}{L} \tag{30}$$

where z = the vertical displacement from the horizontal in the tilted grating, as shown in Figure 13 (for flat gratings, $z = 0$).

Each mapping interval is equal to the length of the grating. In the current shadow moiré road inspection system, the grating length is approximately 86.36 cm (34 in.). Hence, the road inspection vehicle will acquire data at 86.36-cm increments along a road surface, effectively mapping the pavement continuously, without any gaps or overlaps. The

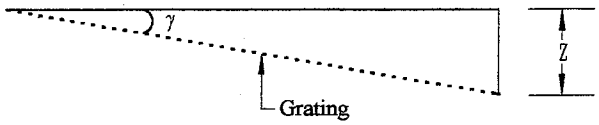

FIGURE 13 Vertical displacement, *Z*.

roughness value for each mapping interval may be obtained as shown in Figure 14. An average roughness value for a span L of road section can be derived from the acquired data.

Binarization Algorithm

This algorithm converts 256 gray-scale images, such as the fringe pattern image shown in Figure 2, into the black-and-white intensity components (*12*), as shown in Figure 15. A binarized image permits faster analysis on both the computer and the image processor. This algorithm uses a statistical pixel intensity analysis to optimize the contrast between fringes and backgrounds. Binarization occurs after the algorithm finds the binarization threshold intensity value (*13*). Pixel

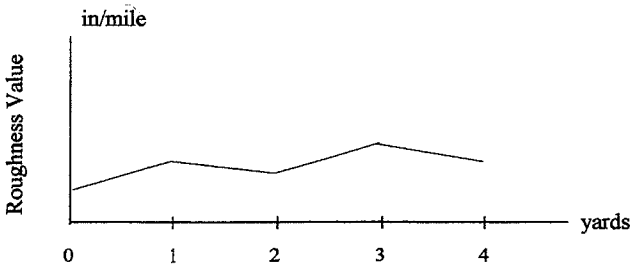

FIGURE 14 Typical roughness values for each mapping interval along a roadway.

FIGURE 15 Black-and-white intensity components of binarize interferogram image.

intensities that fall below the threshold intensity value are converted to black. Intensities that lie above the threshold value are converted to white, resulting in black fringes with white backgrounds. Results of binarization of images acquired during field testing are presented in Table 4.

TABLE 4 Effectiveness of Binarization Algorithm with Various Types of Pavement

Type of Pavement	Performance of Binarization
Light-colored concrete	5
Concrete with surface degradation	5
Dark asphalt	5
Gravel roads	3
Dirt roads	2

Note: 5 = excellent; 4 = very good; 3 = good; 2 = fair; 1 = poor.

Fringe Analysis Algorithm

This algorithm uses binarized images to extract the medial or center line of each fringe (*7*). The resultant image comprises fringes that are uni-pixel in thickness (Figure 16). The thinned fringes are then ordered and processed. Processing involves determining the planar coordinates of each fringe and multiplying the appropriate order index by Δh to determine the vertical displacement of the surface deformation. This leads to a set of three coordinates for any point along a fringe. The operator may choose the number of points along a fringe to process. All three coordinates are written as an ASCII file by the computer and later plotted to obtain a three-dimensional surface distress reconstruction. The effectiveness of this algorithm is related to the quality of binarization of the image.

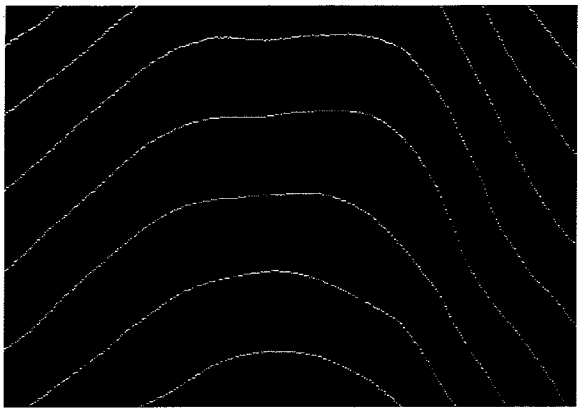

FIGURE 16 Thinned interferogram image.

Road Inspection Software

The road inspection software consists of a user-friendly master program and several small files. This software was written in the C programming language and runs under MS-DOS. The LED tracking, screening, binarization, and fringe analysis algorithms were integrated into the executable road inspection program. The software is a stand-alone tool for analyzing and processing images acquired from the road inspection vehicle. Following are features of the software:

- Processing of images directly from videotape or stored graphics files;
- Image screening, resulting in roughness and change of slope indexes;
- Image binarization (automatic or manual thresholding);
- Extraction of three-dimensional ASCII data for contour plotting;
- LED flash tracking to determine distance traveled;
- Extraction of ASCII screening data including frame code and roadway locations;
- Fast location of LED images by means of point-and-click mouse operation;
- Location of frame codes for videotape playback;
- Location of interferogram boundary edges by means of mouse operation;
- Full VCP control such as field-by-field playback, fast forward, fast reverse, and stop;
- Autoload configuration file; and
- Help screens.

Figure 17 depicts the relationship between the various algorithms.

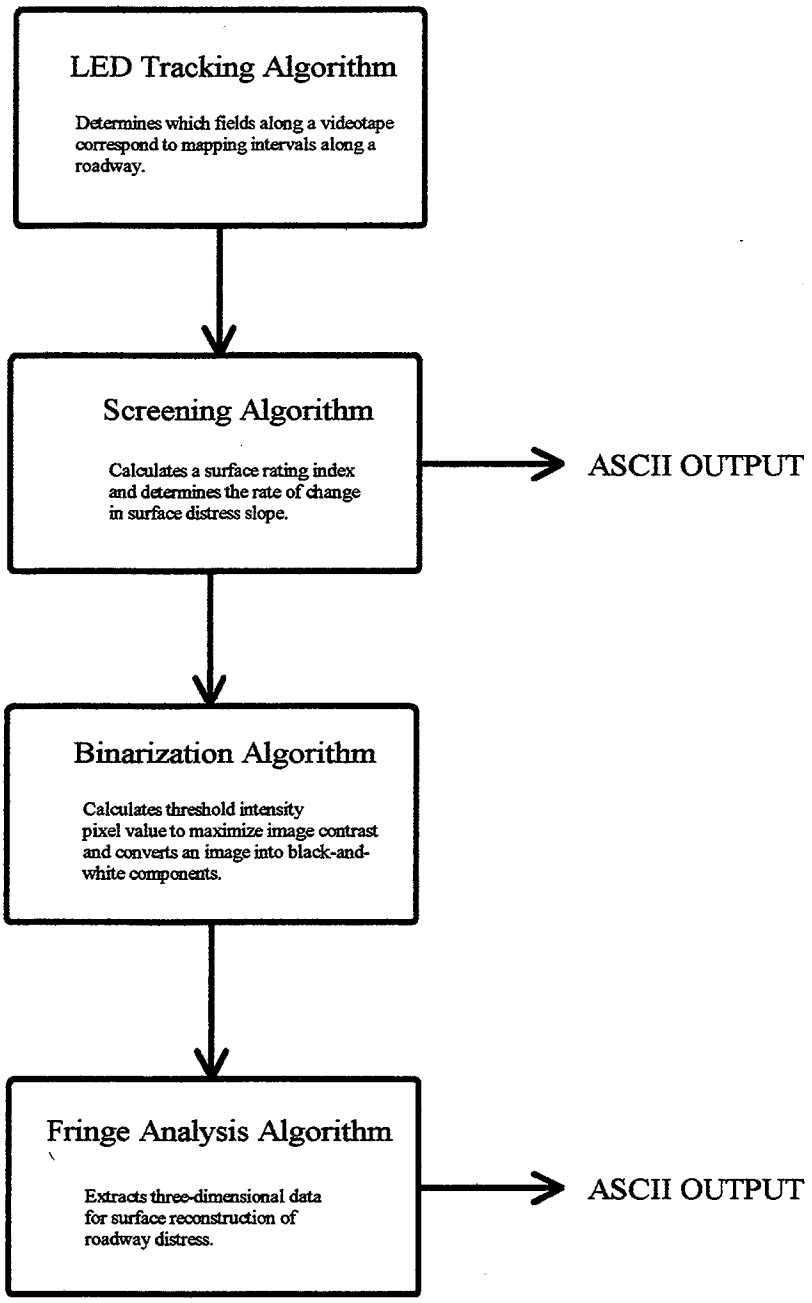

FIGURE 17 Relationship between image processing algorithm sequence.

PLANS FOR IMPLEMENTATION

The road inspection vehicle has been designed to accommodate the needs of the road inspection community. The vehicle is affordable and can acquire large amounts of data at typical highway speeds and requires minimal maintenance and calibration. Implementation of this technology is targeted at small road maintenance organizations, such as those at the county level. It is believed that such organizations would benefit the most from this type of road inspection vehicle because of its modest cost—approximately $60,000—which includes a trailer and all necessary ancillary equipment. The road inspection system is straightforward and simple, thereby eliminating the need for highly trained individuals to operate it. It is expected that both private and county road inspection organizations will realize substantial financial savings in addition to obtaining fast and unbiased road inspection information by using the described shadow moiré road inspection system.

CONCLUSIONS

The field test described in this report has resulted in several advancements and improvements over the original shadow moiré road inspection system. Advancements include a larger and more efficient grating, the ability to conduct road inspection at higher speeds, more accurate distance tracking over severely distressed roadways, a highly optimized lighting system, and the introduction of digital video storage as an alternative to using the U-Matic analog videotape. In addition, user-friendly road inspection software has been written for postanalysis of the videotape. All algorithms originally incorporated into this software were rewritten to make them more efficient and less time-consuming to use when assessing road surface conditions. These advancements have resulted in an affordable and user-friendly road inspection system designed for high-volume data acquisition in connection with automated highway inspection. The shadow moiré road inspection system effectively assesses roadway pavement conditions at velocities up to 88 km/hr (55 mi/hr), regardless of variations in vehicle speed. The resolution of the current system facilitates detection of an 1/8-in. out-of-plane deviation of the road surface. Better resolution is possible by decreasing the pitch of the grating, which is 2 mm in the current version of the road inspection system. Gratings of smaller pitch require very precise workmanship during construction, thereby increasing cost substantially. From the field tests conducted to date, a resolution between 3/16 in. and 1/4 in. results in effective mapping of all significant out-of-plane road surface distresses. Although the use of higher resolutions would result in the acquisition of more surface information, processing time would increase significantly.

Several different sites in northern Illinois were used as testing grounds for the road inspection system. Site selection was based on testing the response of the system to five types of pavement: light-colored concrete, concrete with surface degradation, dark asphalt, gravel roads and dirt roads. The performance of the binarization algorithm is related to the type of pavement, as shown in Table 4. The system performance for assessing surface distresses is, in turn, related to the performance of the binarization algorithm.

The types of surface distress detected by the road inspection system include sagging, rutting, bumps, washboarding, and potholes. Although the shadow moiré system is sensitive to out-of-plane cracking, it usually cannot detect in-plane cracking.

The surface distresses detected by this system have been quantified by means of the roughness and the CSI indexes. Roughness is a measure of the out-of-plane elevation or depression of a road surface in inches divided by the distance traveled by the road inspection vehicle in miles. The CSI index measures the change in slope of the surface being assessed. Both roughness and CSI indexes, and their variations in magnitude along a highway, are written onto the hard disk drive of the host computer. Relative three-dimensional surface dimensions also may be saved on the hard disk for later contour plotting.

The prospect of real-time road surface data processing and reporting is an important consideration. The deployment of fast 32- and 64-bit video processors and CPUs will permit real-time data processing in the future. Such technology will eliminate the need to store shadow moiré interferograms on videotape for later processing of raw data.

The shadow moiré road inspection system eliminates the need for lane closures, eliminates bias in data gathering and analysis, and requires only two individuals, at most, to operate. In addition, the system will provide greater safety for the public and individuals operating the system under typical highway conditions.

REFERENCES

1. Idesawa, M., T. Yatagai, and T. Soma. Scanning Moiré Method and Automatic Measurement of 3-D Shapes. *Applied Optics*, Vol. 16, No. 8, 1977, pp. 2152-2162.

2. Pirodda, L. Shadow and Projection Moiré Techniques for Absolute or Relative Mapping of Surface Shapes. *Optical Engineering*, Vol. 21, No. 4, 1982, pp. 640-649.

3. Meadows, D.M., W.O. Johnson, and J.B. Allen. Generation of Surface Contours by Moiré Patterns. *Applied Optics*, Vol. 9, No. 4, 1970, pp. 942-947.

4. Chiang, C. Moiré Topography. *Applied Optics*, Vol. 14, No. 1, 1973, pp. 177-179.

5. Guralnick, S.A., E.S. Suen, and S. Zoruba. Development of an Automated Pavement Inspection System for the Non-Destructive Evaluation of Highway and Airfield Pavements. In *Research Transformed into Practice: Implementation of NSF Research,* ASCE Press, New York, 1995, pp. 221-232.

6. Jin, G., and S.A. Guralnick. Parametric Investigation of an Automated NDE Pavement Inspection System. *Journal of Experimental Mechanics*, Vol. 34, No. 3, 1994, pp. 256-261.

7. Zoruba, S. *Development of a Road Inspection Vehicle for the Non-Destructive Evaluation of Roadway Pavement Surface.* M.S. thesis, Illinois Institute of Technology, Chicago, 1994.

8. Jaerisch, W., and G. Makosch. Optical Contour Mapping of Surfaces. *Applied Optics*, Vol. 12, No. 7, 1973, pp. 1552-1557.

9. Hegmon, R.R. A Close Look at Road Surfaces. *Public Roads*, Vol. 57, 1993, pp. 4-7.

10. Paterson, W.D.O. International Roughness Index: Relationship to Other Measures of Roughness and Riding Quality. In *Transportation Research Record 1084;* TRB, National Research Council, Washington, D.C., 1986, pp. 49-59.

11. Sayors, M.W., T.D. Gillespie, and C.A.V. Queiroz. The International Road Roughness Experiment: A Basis for Establishing a Standard Scale for Road Roughness Measurements. In *Transportation Research Record 1084*, 1986, pp. 76-85.

12. Otsu, N. A Thresholding Selection Method from Gray-Level Histograms. *IEEE Transactions on Systems, Man and Cybernetics,* Vol. SMC-9, No. 1, 1979, pp. 62-66.

13. Wang, S., and R.M. Haralick. Automatic Multi-threshold Selection. *Computer Vision, Graphics and Image Processing,* Vol. 25, 1984, pp. 46-67.